

Dynamics of a vapor bubble inside a vertical rigid cylinder with and without a deposit rib

A. NOURBAKHS¹⁾, F. ROUZBAHANI²⁾

¹⁾ *Department of Mechanical Engineering
Bu-Ali Sina University
Hamedan, Iran
e-mail nourbakhsh@basu.ac.ir*

²⁾ *Department of Mechanical Engineering
Hamedan branch, Islamic azad University
Hamedan, Iran*

IN THIS PAPER, THE DYNAMICS OF A VAPOUR BUBBLE generated due to local energy input inside a vertical rigid cylinder and in the absence of buoyancy forces was investigated. Different ratios of the diameter of the rigid cylinder up to the maximum radius of the bubble were considered. The boundary integral equation method was employed for numerical simulation of the problem. The results show that during the collapse phase of the bubble inside a vertical rigid cylinder, two liquid micro jets are developed on the top and bottom sides of the vapor bubble and are directed inward. It is found that by increasing the ratio of the cylinder diameter to the maximum radius of the bubble, the rate of the growth and collapse phases of the bubble increases and the lifetime of the bubble decreases. The results also show that an increase in the thickness of the deposit rib inside a vertical rigid cylinder slightly decreases the lifetime of the bubble.

Key words: vapor bubble, vertical rigid cylinder, deposit rib, boundary element method.

Copyright © 2016 by IPPT PAN

1. Introduction

THE DYNAMICS OF A VAPOR BUBBLE generated due to local energy input in the vicinity of different kinds of surfaces is of significant importance in medicine and industry. Numerical and experimental results have shown that a vapor bubble generated due to local energy input in the vicinity of a rigid boundary is attracted towards the rigid surface. In this case, during the collapse phase of the bubble, a liquid micro jet is developed on the side of the bubble farthest from the rigid boundary and is directed towards it [1–3]. Numerical results have also shown that during the growth and collapse of a vapour bubble generated due to

local energy input beneath a free surface, the vapour bubble has different behavior. In this case, the vapor bubble is repelled from the free surface. During the collapse phase, a liquid micro jet is developed on the side of the bubble closest to the free surface and is directed away from it [4–6]. In the case of pulsation of the vapor bubble near a rigid surface, the impingement of the liquid micro jet to the rigid surface is an important cause of mechanical erosion. Experimental investigations also show that at the end of the collapse phase of the vapor bubble and just before its rebound, a shock wave is emitted in the liquid domain. The emission of the shock wave inside the liquid domain is also a cause of rigid surface destruction [7].

A model for the description of the growth and collapse of a vapor bubble in a small tube was presented by YUAN *et al.* [8]. They found that the maximum volume of the bubble and its lifetime depend in a complex way on the channel geometry and the initial energy distribution. The evolution of the bubble in gravity and the jet formation when the charge explodes near a structure were simulated by ZHANG *et al.* [9]. They observed that the oblique jet directed toward the wall is formed under the combined action of the buoyancy (gravity) and the pulling force. GASENKO *et al.* [10] have analyzed the nonlinear dynamics of vapor bubbles for external pressure changing step by step. Primary attention was focused on determining the conditions of complete vapor cavity collapse during the first oscillation periods, depending on three parameters: Peclet number, Jacob number and wave intensity. The influence of viscoelasticity on the dynamics of cavitation bubbles near rigid boundaries was modeled by LIND and PHILLIPS [11]. They indicated that viscoelasticity can serve to suppress the formation of a liquid jet.

In this paper, the dynamics of a vapor bubble inside a vertical rigid cylinder with and without a deposit rib generated due to high local energy input is numerically investigated by employing the boundary integral equation method. Different ratios of the rigid cylinder diameter up to the maximum radius of the bubble and different sizes of the deposit rib are considered. Numerical study on the behavior of a vapor bubble inside a vertical rigid cylinder is of great importance in medicine and industry.

2. Governing equations and numerical method

2.1. Geometrical definition

The vapor bubble is generated due to local energy input inside a vertical rigid cylinder with and without a deposit rib. The problem is axisymmetric. The vertical and radial axes are shown in Fig. 1. The vertical rigid cylinder is assumed to be a long pipe.

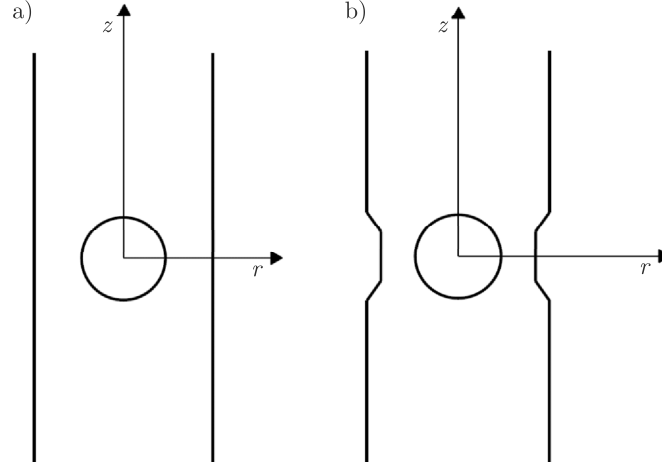


FIG. 1. Schematic representation of the vapor bubble inside a vertical rigid cylinder: a) without a deposit rib, b) with a deposit rib.

2.2. Hydrodynamic equation

The liquid flow around the vapor bubble is assumed to be inviscid, irrotational and incompressible, and the surface tension is neglected. Therefore, the liquid flow around the vapor bubble is a potential flow and Green's integral formula governs the hydrodynamic behavior of this problem.

$$(2.1) \quad C(p)\phi(p) + \int_S \phi(q) \frac{\partial}{\partial n} \left[\frac{1}{|p-q|} \right] dS = \int_S \frac{\partial}{\partial n} [\phi(q)] \left(\frac{1}{|p-q|} \right) dS,$$

where ϕ is the velocity potential and S is the boundary of the liquid domain which includes the bubble boundary and the internal surface of the vertical rigid cylinder, p is any point on the boundary or in the liquid domain and q is any point on the boundary. $C(p)$ is 2π when p is on the boundary and 4π when p is inside the liquid domain.

The unsteady Bernoulli equation in its Lagrangian form is used for calculating the velocity potential at the successive time steps and is given as

$$(2.2) \quad \frac{D\phi}{Dt} = \frac{P_\infty - P_b}{\rho} + \frac{1}{2} |\nabla\phi|^2$$

where P_∞ is pressure in the far field, P_b is pressure inside the vapor bubble, ρ is density and t is time.

2.3. Discretization of the boundaries

The boundary of the vapor bubble is discretized into M cubic spline elements and the internal surface of the vertical rigid cylinder is divided into $2N$ linear segments. The origin of the vertical and radial axes was located at the center of the initial spherical minimum volume of the vapor bubble. The vertical rigid cylinder both upward and downward of the radial axis is discretized up to physical infinity, where the growth and collapse phases of the vapor bubble do not have any considerable effects on the fluid flow. Figure 2 illustrates the discretized representation of the vapor bubble generated due to local energy input inside a vertical rigid cylinder without and with a deposit rib. This figure also shows the discretized internal surface of the vertical rigid surface.

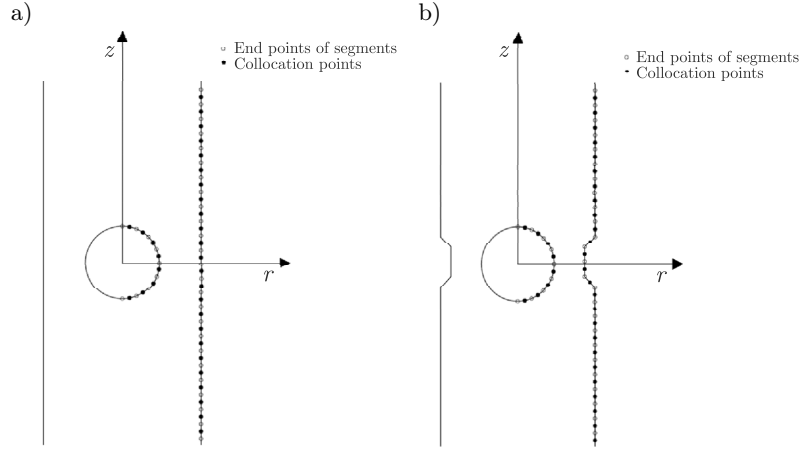


FIG. 2. Discretized representation of the vapor bubble and internal surface of the vertical rigid cylinder in the cases: a) without a deposit rib, b) with a deposit rib.

2.4. Discretization of the equations

Equation (2.3) is a system of linear equations which represents the discretized form of Eq. (2.1):

$$\begin{aligned}
 (2.3) \quad 2\pi\phi(p_i) + \sum_{j=1}^{M+2N} \left\{ \phi(q_j) \int_{S_j} \frac{\partial}{\partial n} \left[\frac{1}{|p_i - q_j|} \right] dS \right\} \\
 = \sum_{j=1}^{M+2N} \left\{ \frac{\partial}{\partial n} [\phi(q_j)] \int_{S_j} \left(\frac{1}{|p_i - q_j|} \right) dS \right\},
 \end{aligned}$$

whereas Eq. (2.4) represents the discretized form of unsteady Bernoulli equation and allows the velocity potential to be time marched over a time increment of Δt .

$$(2.4) \quad [\phi_i]_{t+\Delta t} = [\phi_i]_t + \Delta t \left\{ \frac{P_\infty - P_b}{\rho} + \frac{1}{2} |\nabla \phi|^2 \right\}.$$

2.5. Evolution of the vapor bubble

A variable time increment is defined as

$$(2.5) \quad \Delta t = \min \left| \frac{\Delta \phi}{\frac{P_\infty - P_c}{\rho} + \frac{1}{2}(\psi^2 + \eta^2)} \right|,$$

where $\Delta \phi$ is a constant and represents the maximum increment of the velocity potential between two successive time steps. Additionally, P_c is saturated vapor pressure, ψ is normal velocity on the boundary of the liquid domain and η is tangential velocity.

The original formula and numerical method were described in detail by DADVAND *et al.* [12], SHERVANI-TABAR *et al.* [6, 13], and SALEKI-HASELGHOUBI *et al.* [14], and only a brief outline is given in this paper.

At the beginning of calculations, the vapor bubble has a minimum spherical volume with a very high pressure inside. The mathematical model for predicting the initial minimum radius of the bubble and the corresponding pressure inside is based on the Rayleigh equation [15], which was developed by BEST [16]. The details of the calculations for specifying initial values of the bubble volume and its inside pressure were given by SHERVANI-TABAR *et al.* [17]. The normal derivative of the velocity potential and the velocity potential on the bubble boundary at the beginning of the calculations are known and are equal to zero. Normal velocity on the boundary of the vertical rigid cylinder is also known and is equal to zero. Therefore, the linear system of equations (2.3) was solved by employing the Gauss elimination method. Consequently, the normal velocity on the bubble boundary and the velocity potential on the internal surface of the vertical rigid cylinder are found. Having the distribution of the velocity potential on the bubble boundary, the tangential velocity on the bubble boundary is obtained by differentiating the velocity potential on the bubble surface with respect to its arc length. Having the normal and tangential velocity on the bubble boundary, radial and vertical components of the velocity on the bubble boundary are obtained. Since the radial and vertical components of the velocity on the bubble boundary are known, by employing a second order Runge-Kutta scheme, the evolution of the vapor bubble over a time increment of Δt is obtained. In addition, by using the discretized form of Bernoulli equation, the distribution of the velocity potential over the bubble surface at the next time step is calculated.

2.6. Non-dimensional parameters

The problem under investigation is non-dimensionalized by employing the maximum radius of the bubble R_m , diameter of the vertical rigid cylinder D , liquid density ρ , pressure in the far field P_∞ and saturated vapor pressure P_c . The non-dimensional parameters which are used in this paper are defined as

$$(2.6) \quad \lambda = \frac{D}{R_m},$$

$$(2.7) \quad t = \frac{t}{R_m} \left(\frac{P_\infty - P_c}{\rho} \right)^{1/2},$$

$$(2.8) \quad \Psi = \psi \left(\frac{\rho}{P_\infty - P_c} \right)^{1/2}.$$

3. Numerical results and discussion

Numerical results were obtained in two parts. In part 3.1, the vapor bubble was generated due to local energy input inside a vertical rigid cylinder without a deposit rib, and in part 3.2, the vapor bubble was generated due to local energy input inside a vertical rigid cylinder with a deposit rib.

3.1. A vapor bubble inside a vertical rigid cylinder without a deposit rib

Figure 3 illustrates the growth and collapse phases of a vapor bubble generated due to local energy input inside a vertical rigid cylinder with $\lambda = 3$. Figure 3a shows that during its growth phase the vapor bubble elongates symmetrically in the vertical direction. This phenomenon is due to the effects of the rigid cylinder wall. The rigid cylinder wall prevents the expansion of the bubble along the radial axis, and since the top and bottom sides of the bubble are free to move upwards and downwards respectively, the vapor bubble elongates in the vertical direction. Consequently, the velocity of the bubble boundary along its top and bottom sides is higher than the velocity of the bubble boundary in the vicinity of the rigid cylinder wall. Therefore, the fluid particles adjacent to the top and bottom sides of the bubble had greater dynamic pressure with respect to the fluid particles in the vicinity of the rigid boundary. At the end of the bubble growth phase, the dynamic pressure in the liquid domain converts to the static pressure. Thus, at the early stages of the collapse phase of the bubble, the static pressure of the fluid regions adjacent to the top and bottom sides of the bubble was greater than the static pressure of the fluid region between the bubble and the rigid cylinder wall. Therefore, during the collapse phase of the bubble, the high static pressure on the fluid regions adjacent to the top and bottom sides of the bubble causes the development of two broad liquid micro

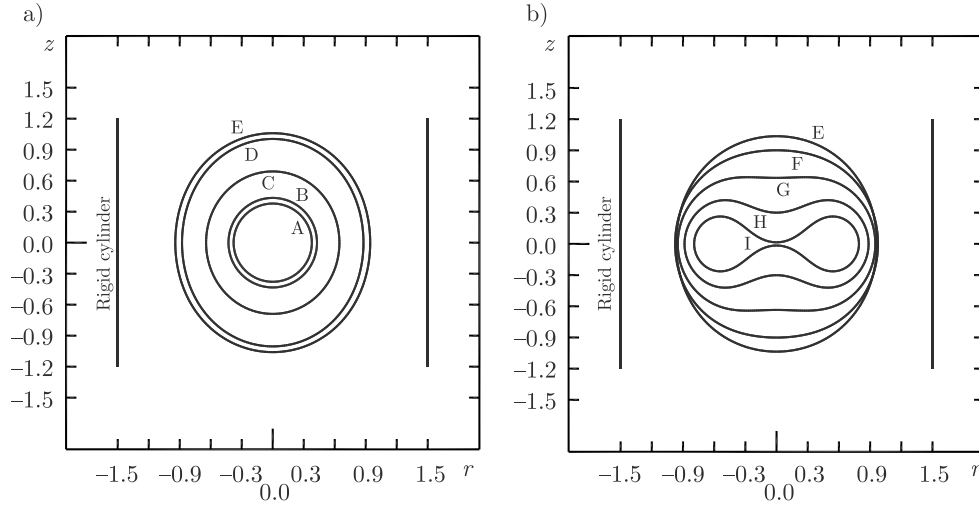


FIG. 3. Growth and collapse of a single vapor bubble inside a vertical rigid cylinder in the absence of buoyancy forces with $\lambda = 3$; a) growth phase: A) 0.00364, B) 0.12644, C) 0.50345, D) 1.42588, E) 2.46031; b) collapse phase: E) 2.46031, F) 3.09105, G) 3.68906, H) 4.17126, I) 4.51301.

jets on the top and bottom sides of the bubble, which are directed inwards (as illustrated in Fig. 3b). The formation of the liquid jet was also observed experimentally during the collapse of spark-generated bubbles near a horizontal rigid flat plate by ZHANG *et al.* [18]. A numerical study of the dielectric liquid around an electrical discharge-generated vapor bubble was performed by SHERVANI-TABAR and MOBADERSANY [13]. They found that the vapor bubble remains almost spherical during its growth phase. During the collapse phase, the vapor bubble elongates in the direction perpendicular to the parallel boundaries of the tool and the workpiece. They also found that at the last stages of the collapse phase, an annular liquid jet develops around the bubble and the bubble takes the shape of twin necked bulbs.

Figures 4 and 5 show that by decreasing the ratio of the vertical rigid cylinder diameter to the maximum radius of the bubble λ , elongation of the vapor bubble during its growth phase is more significant in the vertical direction.

A comparison between Fig. 3 and Fig. 5 shows that the liquid micro jets in the case of Fig. 3 are much broader. Thus, it should be noted that by increasing λ , the liquid micro jets which were developed on the top and bottom sides of the bubble become broader. In other words, by decreasing λ , the effect of the rigid cylinder on the bubble behavior during its growth and collapse phases increases and consequently causes the development of two narrower liquid micro jets on the top and bottom sides of the bubble (this is in agreement with the results

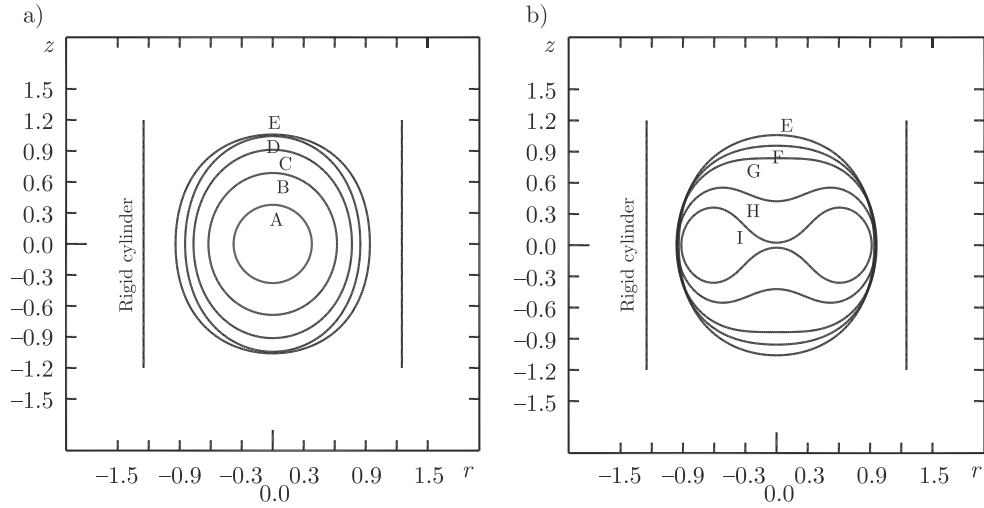


FIG. 4. Growth and collapse of a single vapor bubble inside a vertical rigid cylinder in the absence of buoyancy forces with $\lambda = 2.5$; a) growth phase: A) 0.00364, B) 0.50912, C) 1.01104, D) 1.51611, E) 2.68085; b) collapse phase: E) 2.68085, F) 3.11222, G) 3.42825, H) 4.12248, I) 4.63623.

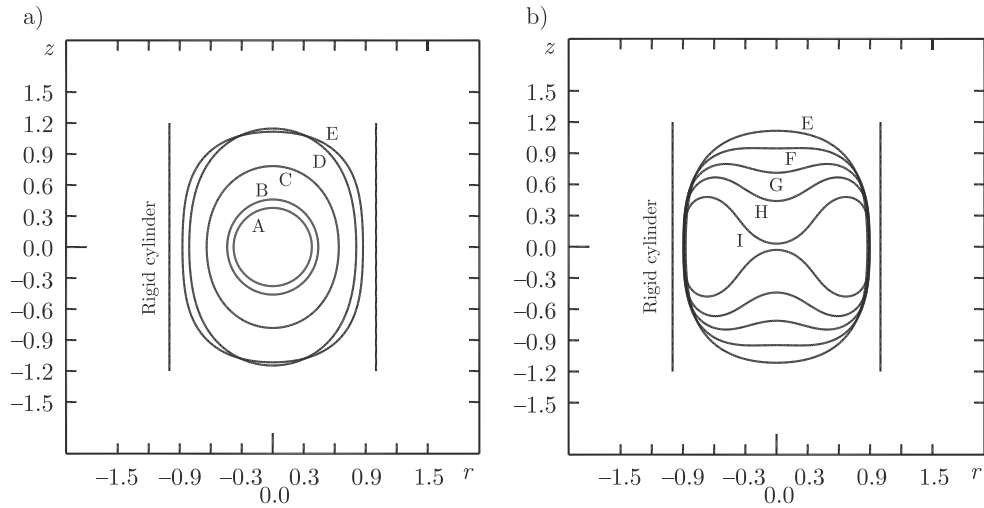


FIG. 5. Growth and collapse of a single vapor bubble inside a vertical rigid cylinder in the absence of buoyancy forces with $\lambda = 2$; a) growth phase: A) 0.00364, B) 0.17783, C) 0.67053, D) 1.76091, E) 2.89102; b) collapse phase: E) 2.89102, F) 3.40912, G) 3.85424, H) 4.25939, I) 4.81757.

obtained by HAJIZADEH AGHDAM *et al.* [19]). YUAN *et al.* [8] found that the maximum volume of the bubble and its lifetime depend in a complex way on the channel geometry.

The validity of our numerical study can also be verified by the results of ISHIDA *et al.* [20]. They studied experimentally the cavitation bubble behavior between two solid parallel walls. They showed that the bubble between the walls maintains its spherical shape and reaches the maximum volume. Therefore, the bubble laterally shrinks and forms a dumbbell-shaped bubble.

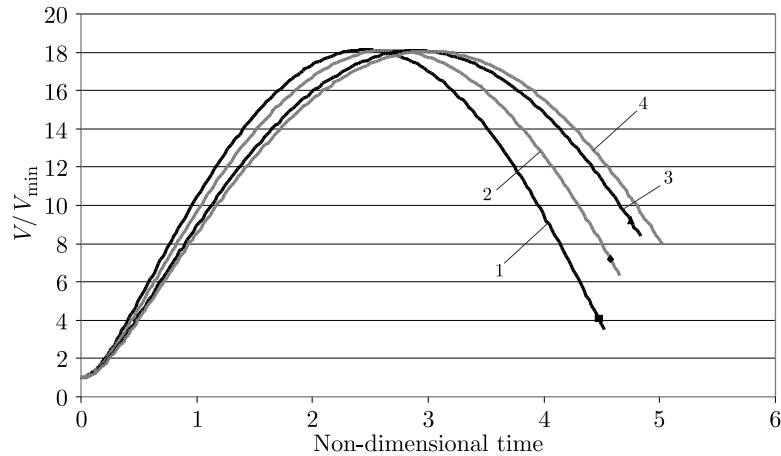


FIG. 6. Variation of rational volume of the bubble in the absence of buoyancy forces against non-dimensional time in the cases of: (1) $\lambda=3$, (2) $\lambda=2.5$, (3) $\lambda=2$, (4) $\lambda=1.75$.

Figure 6 illustrates the variation of the non-dimensional volume of the bubble with respect to non-dimensional time. It shows that the vapor bubble expands to the largest maximum volume and the lifetime of the bubble (the time interval between the initial spark and the toroidal bubble formation) is the longest. This, in turn, makes the pressure inside the bubble to decrease rapidly to the lowest magnitude (this is in agreement with the numerical study by SALEKI-HASELGHOUBI *et al.* [14]). Figure 7 also shows that by increasing λ , the rate of the growth and collapse of a vapor bubble inside a vertical rigid cylinder becomes higher and the lifetime of the bubble becomes shorter. Therefore, by decreasing λ , the effect of the rigid cylinder on the behavior of the bubble is more considerable and increases the lifetime of the bubble. This is in agreement with the experiment by HAJZADEH AGHDAM *et al.* [19]. They showed the bubble lifetime for different values of λ , and found that for larger bubbles (i.e., smaller values of λ), there is an increase of the bubble lifetime.

Figure 7 illustrates the variation of internal pressure of the vapor bubble inside a vertical rigid cylinder in the cases in Fig. 6. It should be noted that for the purpose of increasing the lifetime of the bubble, the pressure at the far field is assumed to be 5000 Pa. This assumption also makes the buoyancy forces to be

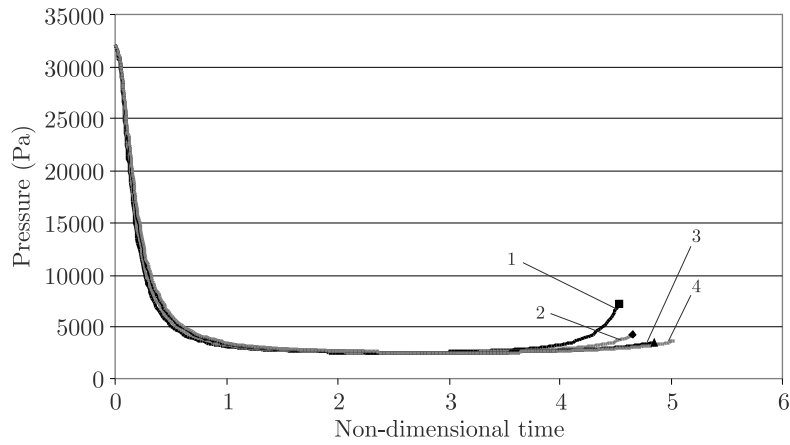


FIG. 7. Variation of internal pressure of a single cavitation bubble inside a vertical rigid cylinder against non-dimensional time in the absence of buoyancy forces in the cases of: (1) $\lambda=3$, (2) $\lambda=2.5$, (3) $\lambda=2$, (4) $\lambda=1.75$.

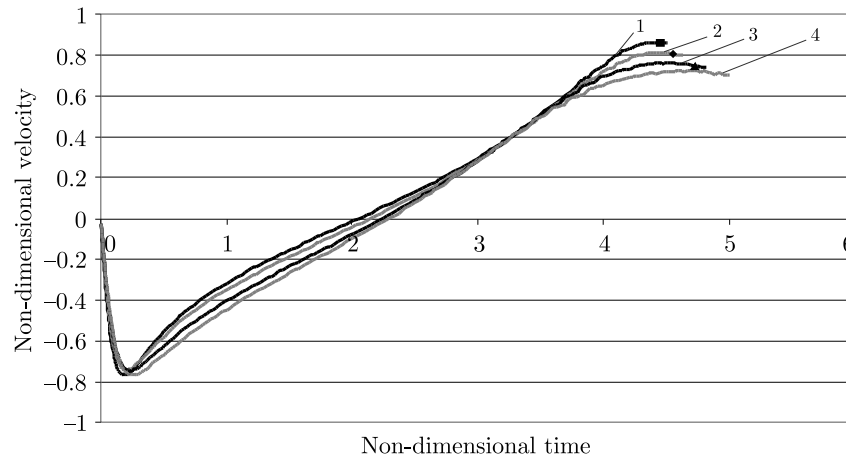


FIG. 8. Variation of non-dimensional velocity of liquid jets in the absence of buoyancy forces against non-dimensional time in the cases of: (1) $\lambda=3$, (2) $\lambda=2.5$, (3) $\lambda=2$, (4) $\lambda=1.75$.

more substantial. A numerical study on the dynamics of a buoyant vapor bubble inside a vertical rigid cylinder will be our future work.

Figure 8 shows that by increasing λ , the velocity of the liquid micro jets at the latest stages of the collapse phase becomes higher.

Figure 9a illustrates the variation of the pressure at the intersection of the radial axis with the internal surface of the vertical rigid cylinder with respect to non-dimensional time, while Fig. 9b shows the variation of pressure at the inter-

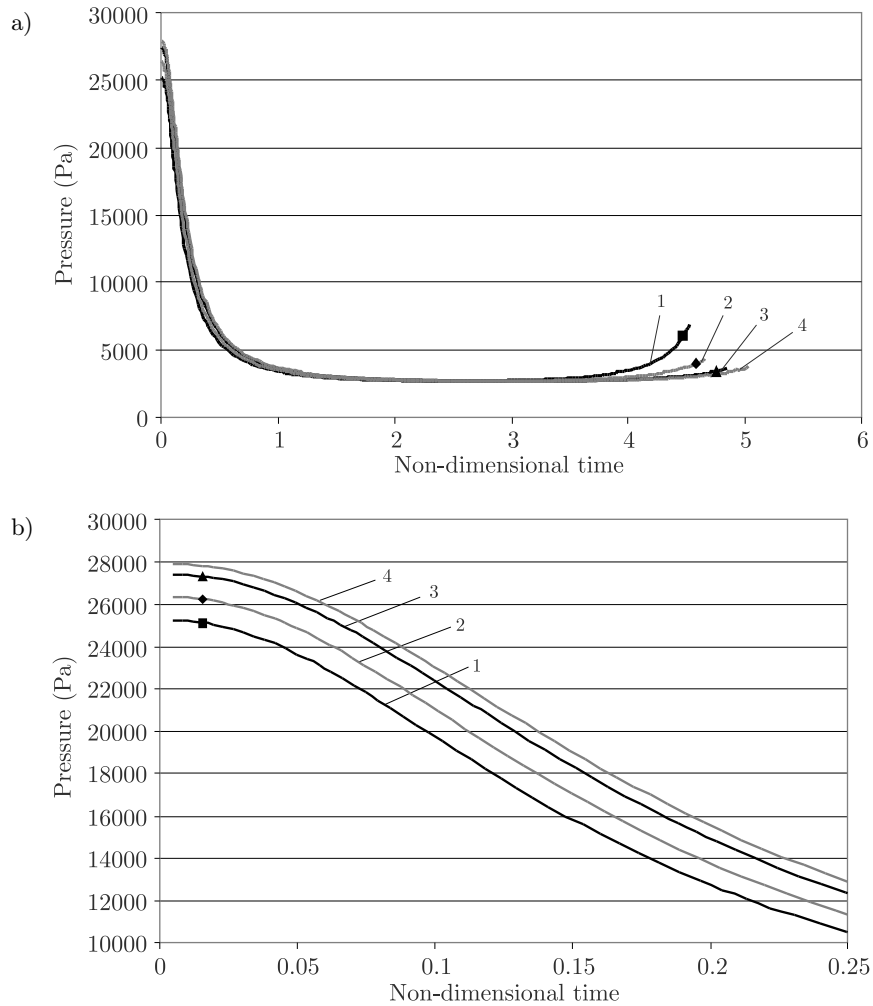


FIG. 9. a) Variation of pressure at the intersection point of radial axis with internal surface of the vertical rigid cylinder against non-dimensional time in the absence of buoyancy forces in the cases of: (1) $\lambda = 3$, (2) $\lambda = 2.5$, (3) $\lambda = 2$, (4) $\lambda = 1.75$. b) Variation of pressure at the intersection point of radial axis and internal surface of the vertical rigid cylinder against non-dimensional time in the absence of buoyancy forces in the cases of: (1) $\lambda = 3$, (2) $\lambda = 2.5$, (3) $\lambda = 2$, (4) $\lambda = 1.75$.

section of the radial axis with the internal surface of the vertical rigid cylinder against non-dimensional time at the early stages of the bubble growth phase.

3.2. A vapor bubble inside a vertical rigid cylinder with a deposit rib

In this section, two types of deposit rib inside the vertical rigid cylinder are considered as the first type and the second type of deposit rib. Figure 10

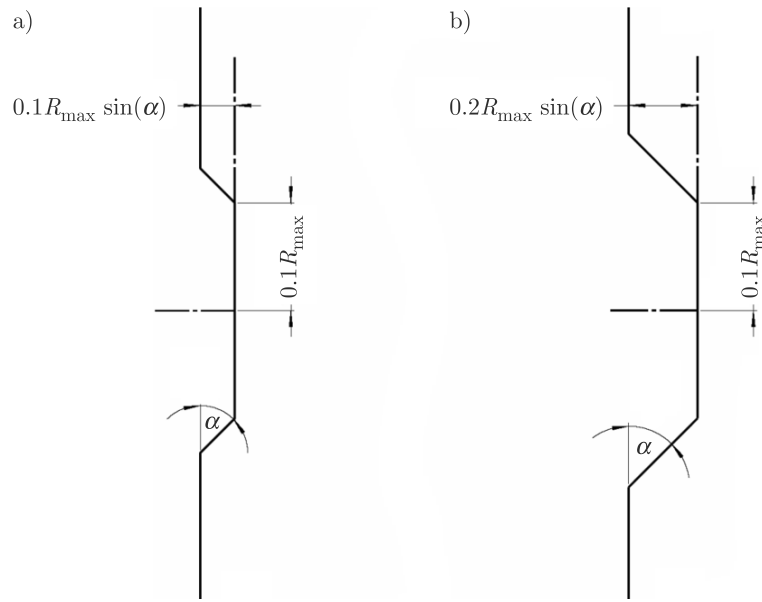


FIG. 10. Geometrical characteristics of the: a) first and b) second type of deposit rib inside the vertical rigid cylinder.

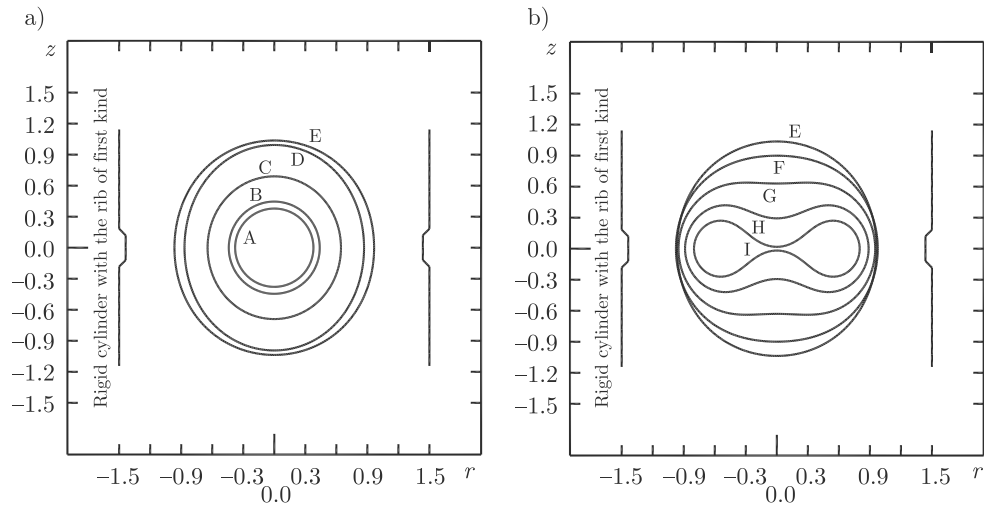


FIG. 11. Growth and collapse of a single vapor bubble inside a vertical rigid cylinder with a deposit rib of the first type in the absence of buoyancy forces with $\lambda = 3$; a) growth phase: A) 0.00364, B) 0.14384, C) 0.50346, D) 1.36254, E) 2.46015; b) collapse phase: E) 2.46015, F) 3.09044, G) 3.68707, H) 4.16801, I) 4.49676.

illustrates the geometrical characteristics of the first type and the second type of deposit rib inside the vertical rigid cylinder.

Figure 11 illustrates the growth and collapse of a vapor bubble generated due to local energy input inside a vertical rigid cylinder with a deposit rib of the first type. As it is shown in Fig. 11a, the vapor bubble during its growth phase elongates in the vertical direction. During the collapse phase, two broad liquid micro jets were developed on top and bottom sides of the vapor bub-

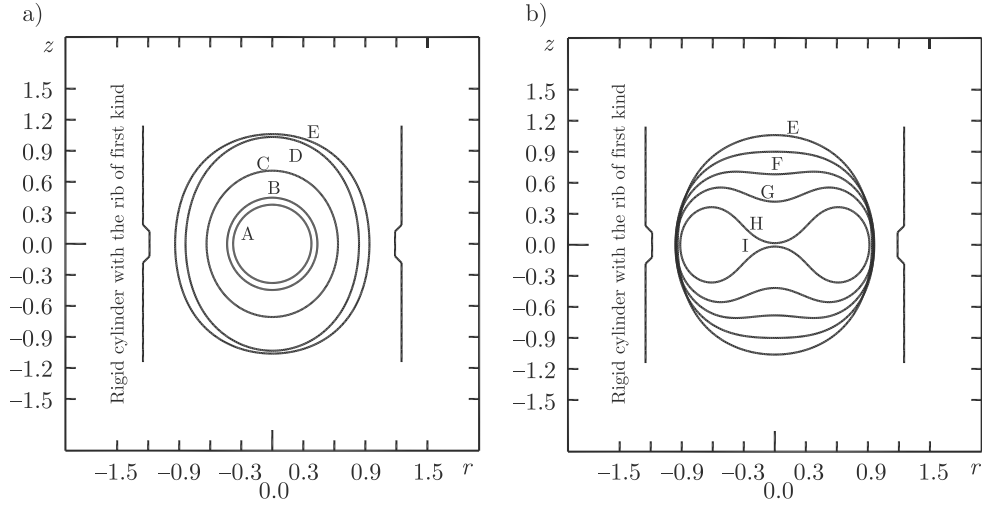


FIG. 12. Growth and collapse of a single vapor bubble inside a vertical rigid cylinder with a deposit rib of the first type in the absence of buoyancy forces with $\lambda = 2.5$; a) growth phase: A) 0.00364, B) 0.15202, C) 0.54476, D) 1.45129, E) 2.67847; b) collapse phase: E) 2.67847, F) 3.26957, G) 3.71969, H) 4.11747, I) 4.63179.

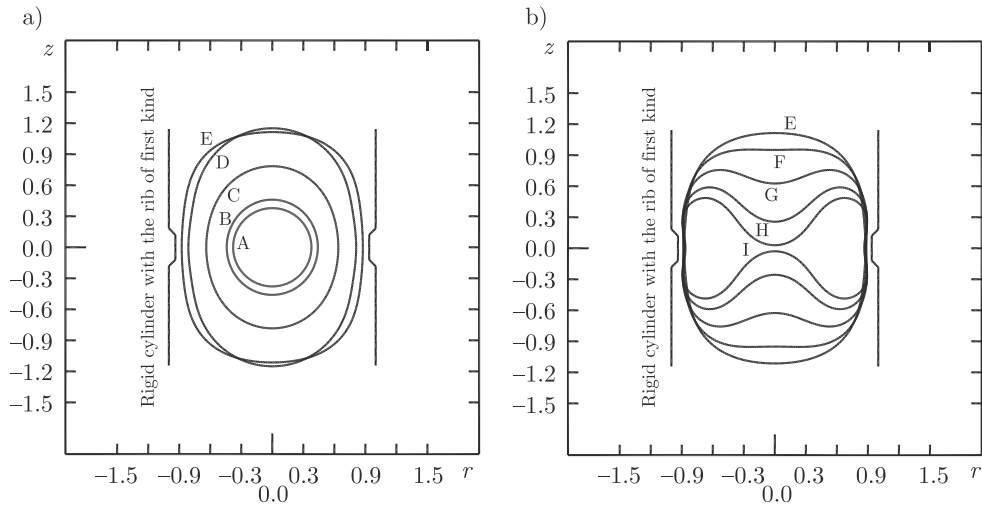


FIG. 13. Growth and collapse of a single vapor bubble inside a vertical rigid cylinder with a deposit rib of the first type in the absence of buoyancy forces with $\lambda = 2$; a) growth phase: A) 0.00364, B) 0.17767, C) 0.66813, D) 1.75528, E) 2.91754; b) collapse phase: E) 2.91754, F) 3.40211, G) 3.98567, H) 4.50366, I) 4.8100.

ble and directed inward. When the bubble reached its maximum volume, the pressure inside the bubble was less than the pressure outside and the pressure of the liquid domain increased by moving far away from the bubble. Also, at the instant of the maximum volume of the bubble, the fluid near the walls in the domain was escaping away from the bubble due to bubble expansion and was directed toward the bubble at the center of the gap. After this, the bubble was going to disintegrate because of the higher pressure outside the bubble. Next, a lateral high-pressure region developed in the middle of the gap close to the bubble which caused the development of a liquid jet around the bubble. As times went on, the high pressure region closed to the bubble and at the last stages of the collapse phase, a high pressure region appeared just close to the jet of the bubble. A comparison between Fig. 3 and Fig. 11 shows that the existence of a deposit rib of the first type decreases the life-time of the bubble very slightly.

Figures 12 and 13 in comparison with Figs. 4 and 5 show that the lifetime of the bubble inside a vertical rigid cylinder in the presence of a deposit rib of the first type became slightly shorter.

Figures 14, 15 and 16 illustrate the growth and collapse phases of a vapor bubble generated due to local energy input inside a vertical rigid cylinder and in the presence of a deposit rib of the second type. These figures, in comparison with Figs. 11, 12, and 13, show that an increase in the thickness of the deposit rib inside a vertical rigid cylinder also slightly decreases the lifetime of

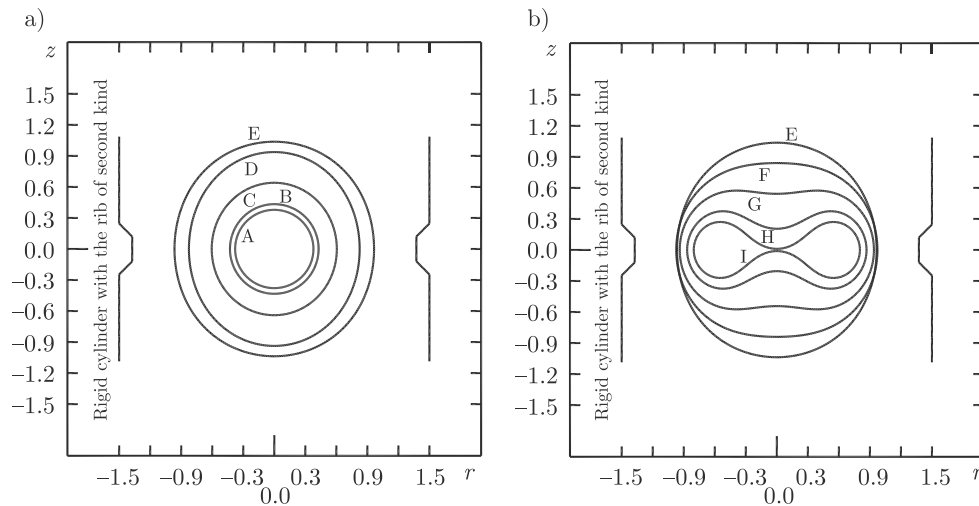


FIG. 14. Growth and collapse of a single vapor bubble inside a vertical rigid cylinder with a deposit rib of the second type in the absence of buoyancy forces with $\lambda = 3$; a) growth phase: A) 0.00364, B) 0.12646, C) 0.41743, D) 1.11871, E) 2.4603; b) collapse phase: E) 2.4603, F) 3.24762, G) 3.81712, H) 4.26443, I) 4.49373.

the bubble. DADVAND *et al.* [12] demonstrated that the wall of the chamber strongly influences the behavior of the bubble. SALEKI-HASELGHOUBI *et al.* [14] investigated the effect of geometry on the bubble behavior. They found that when the rigid boundary and free surface are present simultaneously, the bubble

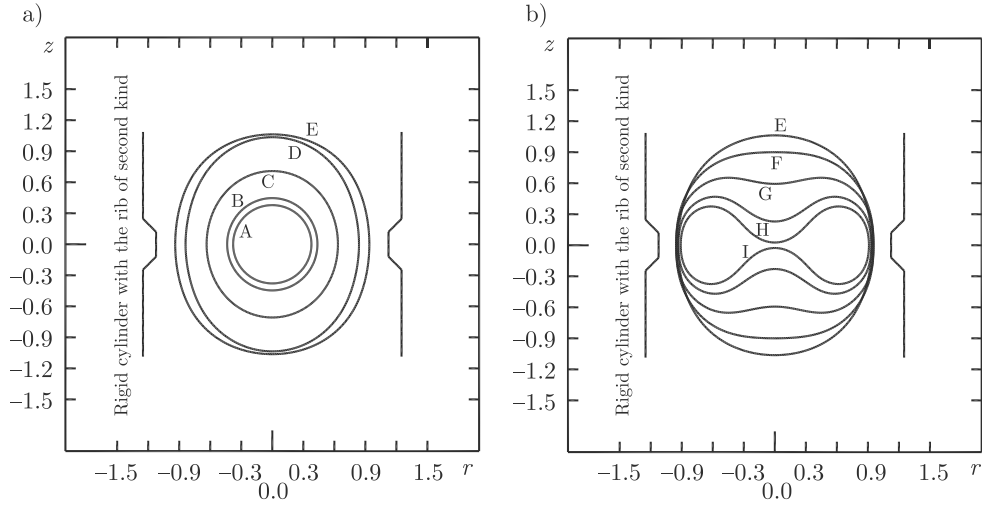


FIG. 15. Growth and collapse of a single cavitation bubble inside a vertical rigid cylinder with a deposit rib of the second type in the absence of buoyancy forces with $\lambda = 2.5$; a) growth phase: A) 0.00364, B) 0.15199, C) 0.54422, D) 1.44975, E) 2.67649; b) collapse phase: E) 2.67649, F) 3.26705, G) 3.85417, H) 4.35067, I) 4.60796.

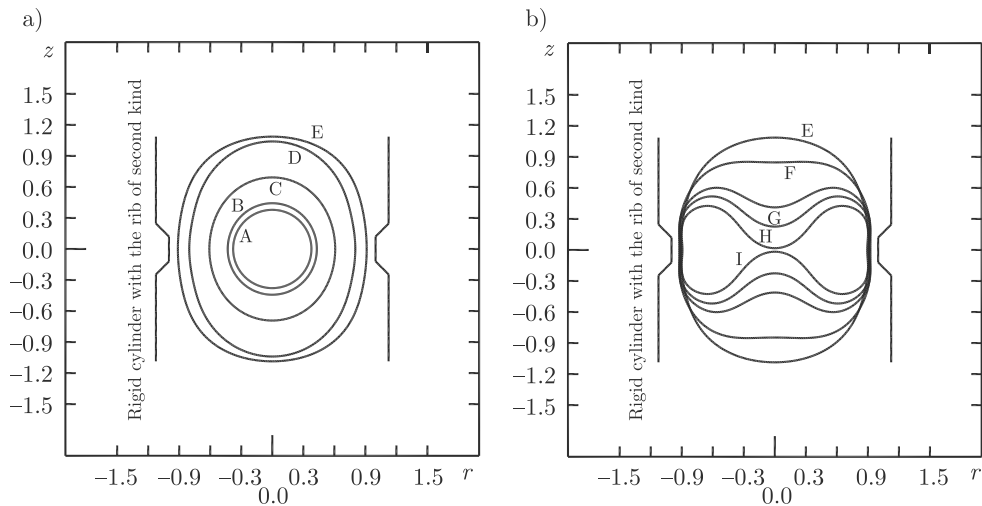


FIG. 16. Growth and collapse of a single cavitation bubble inside a vertical rigid cylinder with a deposit rib of the second type in the absence of buoyancy forces with $\lambda = 2.25$; a) growth phase: A) 0.00364, B) 0.14988, C) 0.51509, D) 1.3728, E) 2.7846; b) collapse phase: E) 2.7846, F) 3.49228, G) 4.18307, H) 4.42763, I) 4.69922.

lifetime depends on the amount of effect each of these boundaries has on the bubble behavior.

Figure 17 illustrates the variation of the internal pressure of the vapor bubble with respect to non-dimensional time. It is seen that, in all the cases, the pressure decreased sharply at the initial stages of the growth phase and remained almost unchanged for a long time during both the growth and collapse phases. Then, the pressure increased sharply at the end of collapse phase, implying that the bubble tends to rebound. It should be noted that for the purpose of increasing the lifetime of the bubble, the pressure at the far field is assumed to be 5000 Pa. As stated earlier, this assumption not only increases the lifetime of the bubble, but also causes the buoyancy forces to be more significant in the case of a buoyant vapor bubble whose dynamics inside a vertical rigid cylinder will be the subject of our future investigation.

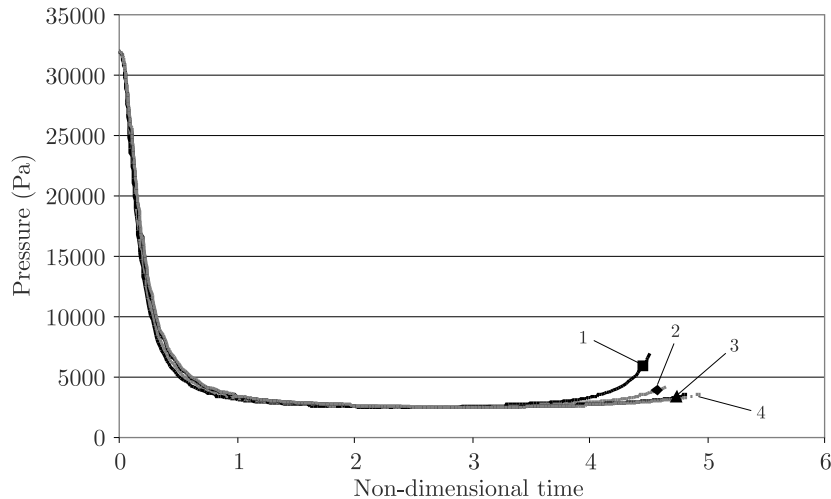


FIG. 17. Variation of internal pressure of a single vapor bubble inside a vertical rigid cylinder with a deposit rib of the first type against non-dimensional time in the absence of buoyancy forces and in the cases of: (1) $\lambda=3$, (2) $\lambda=2.5$, (3) $\lambda=2$, (4) $\lambda=1.85$.

Figure 18 shows the variation of the non-dimensional velocity of liquid micro jets with respect to non-dimensional time when the vapor bubble was inside a vertical rigid cylinder with different values of λ . A comparison between Fig. 8 and Fig. 18 illustrates that the presence of a deposit rib of the first type does not have a considerable effect on the non-dimensional velocity of the liquid micro jets.

Figure 19 illustrates the variation of the pressure at the intersection of the radial axis and internal surface of the vertical rigid cylinder with respect to non-dimensional time in the case of Figs. 11, 12 and 13.

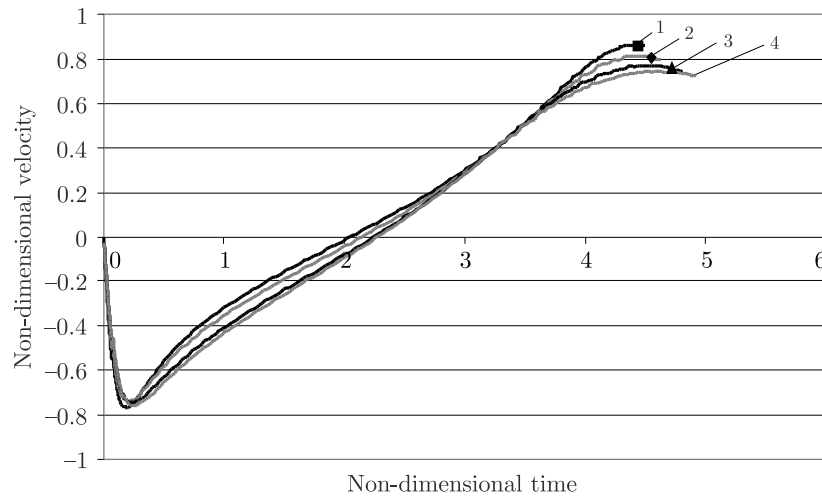


FIG. 18. Variation of non-dimensional velocity of liquid jets on top and bottom sides of the bubble inside a vertical rigid cylinder with a deposit rib of the first type in the absence of buoyancy forces against non-dimensional time and in the cases of: (1) $\lambda=3$, (2) $\lambda=2.5$, (3) $\lambda=2$, (4) $\lambda=1.85$.

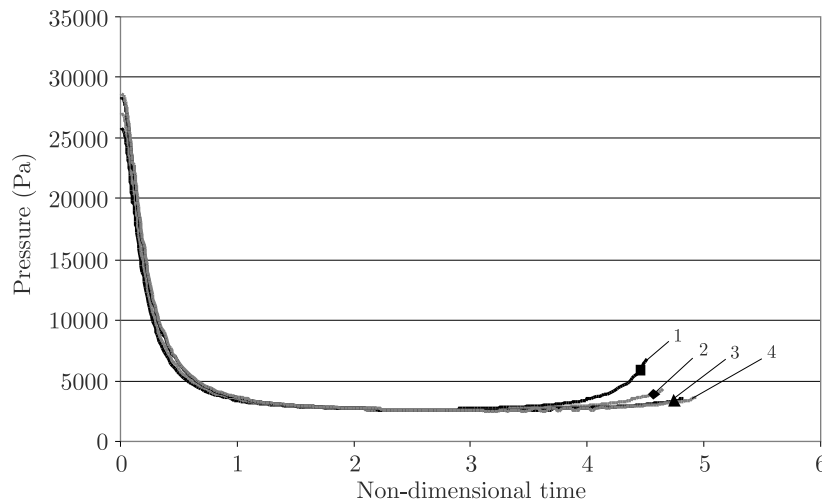


FIG. 19. Variation of pressure at the intersection point of the radial axis and internal surface of the vertical rigid cylinder with a deposit rib of the first type in the absence of buoyancy forces against non-dimensional time and in the cases of: (1) $\lambda=3$, (2) $\lambda=2.5$, (3) $\lambda=2$, (4) $\lambda=1.85$.

Figure 20 illustrates the variation of the pressure at the intersection of the radial axis and internal surface of the vertical cylinder with respect to non-dimensional time in the case of Figs. 14, 15 and 16. It should be noted that in the case of Figs. 14, 15 and 16, the second type of deposit rib was considered.

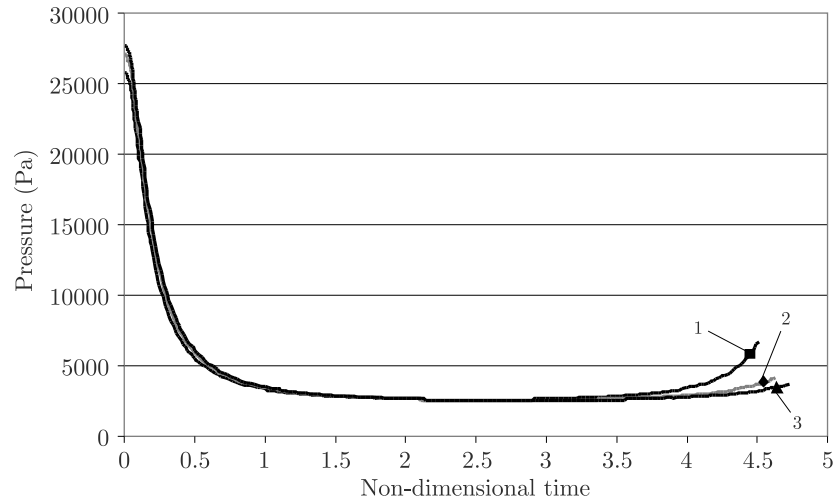


FIG. 20. Variation of pressure at the intersection point of the radial axis and internal surface of the vertical rigid cylinder with a deposit rib of the second type in the absence of buoyancy forces against non-dimensional time and in the cases of: (1) $\lambda=3$, (2) $\lambda=2.5$, (3) $\lambda=2.25$.

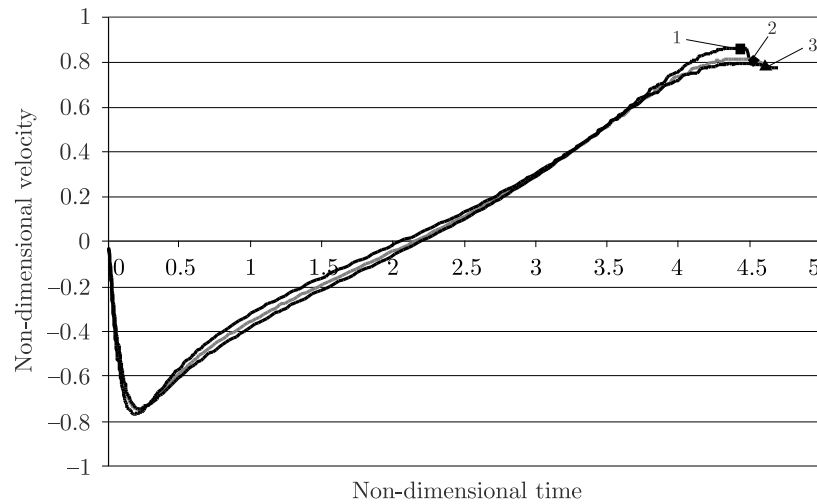


FIG. 21. Variation of non-dimensional velocity of liquid jets on top and bottom sides of the bubble inside a vertical rigid cylinder with a deposit rib of the second type in the absence of buoyancy forces against non-dimensional time and in the cases of: (1) $\lambda=3$, (2) $\lambda=2.5$, (3) $\lambda=2.25$.

Figure 21 illustrates the variation of non-dimensional velocity of the liquid micro jets in the presence of a deposit rib of the second type. A comparison between Fig. 18 and Fig. 21 shows that an increase in the thickness of the deposit rib on the internal surface of the vertical rigid cylinder slightly increases

the velocity of the liquid micro jets on top and bottom sides of the bubble at the latest stages of the bubble collapse phase.

The validity of our numerical study can also be verified by the results of HAJIZADEH AGHDAM *et al.* [19]. Their experimental study concerned the dynamics of an oscillating bubble in a vertical rigid tube. Unfortunately, there are several principal differences between the conditions of the present research and the conditions of their experimental work [19]. Probably the most important difference is that in this experimental work, the effect of buoyancy was considered.

4. Conclusion

In this paper, the dynamic behavior of a vapor bubble generated due to local energy input in the absence of buoyancy forces was numerically investigated by employing a boundary integral equation method.

Numerical results show that during its growth phase the vapor bubble elongates in the vertical direction. During the collapse phase of the bubble, two broad liquid micro jets are developed on the top and bottom sides of the bubble and are directed inward.

Results also showed that by increasing λ , the ratio of the cylinder diameter to the maximum radius of the bubble, the rate of growth and collapse of the vapor bubble inside a vertical rigid cylinder becomes higher and the lifetime of the bubble becomes shorter.

It was found that an increase in the thickness of the deposit rib inside a vertical rigid cylinder also slightly decreases the lifetime of the bubble.

It was also found that an increase in the thickness of the deposit rib on the internal surface of the vertical rigid cylinder slightly increases the velocity of the liquid micro jets on the top and bottom sides of the bubble at the latest stages of the bubble collapse phase.

References

1. J.R. BLAKE, B.B. TAIB, G. DOHERTY, *Transient cavities near boundaries. Part 1. Rigid boundary*, J. Fluid Mech., **170**, 479, 1986.
2. J.R. BLAKE, D.C. GIBSON, *Cavitation bubbles near boundaries*, Ann. Rev. Fluid Mech., **19**, 99–123, 1987.
3. W.K. SOH, M.T. SHERVANI-TABAR, *Computer model for a pulsating bubble near a rigid surface*, Computational Fluid Dynamics Journal, **3**, 1, 223–236, 1994.
4. J.R. BLAKE, B.B. TAIB, G. DOHERTY, *Transient cavities near boundaries. Part 2. Free surface*, J. Fluid Mech., **181**, 197–212, 1986.
5. J.R. BLAKE, D.C. GIBSON, *Growth and collapse of a vapor cavity bubble near a free surface*, J. Fluid Mech., **111**, 123–140, 1981.

6. M.T. SHERVANI-TABAR, *Computer study of a cavity bubble near a rigid boundary, a free surface, and a compliant wall*, PhD Thesis, University of Wollongong, Wollongong, Australia, 1995.
7. W. LAUTERBORN, *Cavitation and coherent optics. Cavitation and inhomogenities in underwater acoustics*, Proceedings of the First International Conference, Göttingen, Germany, Lauterborn (ed.), Springer, 3–12, 1980.
8. H. YUAN, H.N. OĞUZ, A. PROSPERETTI, *Growth and collapse of a vapor bubble in a small tube*, Int. J. Heat Mass Transfer, **42**, 19, 3643–3657, 1999.
9. A. ZHANG, Y. XIONGLIANG, L. JIA, G. JUN, *Comparison between the 3D numerical simulation and experiment of the bubble near different boundaries*, Science in China Series G: Physics, Mechanics & Astronomy, **51**, 12, 1914–1925, 2008.
10. V.G. GASENKO, V.P. ILYIN, V.E. NAKORYAKOV, *Numerical analysis of the dynamics of vapor bubbles*, J. Eng. Thermophysics, **19**, 4, 272–281, 2010.
11. S.J. LIND, T.N. PHILLIPS, *The influence of viscoelasticity on the collapse of cavitation bubbles near a rigid boundary*, Theor. Comput. Fluid Dyn., **26**, 245–277, 2012.
12. A. DADVAND, B.C. KHOO, M.T. SHERVANI-TABAR, S. KHALILPOURAZARY, *Boundary element analysis of the droplet dynamics induced by spark-generated bubble*, Engineering Analysis with Boundary Elements, **36**, 1595–1603, 2012.
13. M.T. SHERVANI-TABAR, N. MOBADERSANY, *Numerical study of the dielectric liquid around an electrical discharge generated vapor bubble in ultrasonic assisted EDM*, Ultrasonics, **53**, 943–955, 2013.
14. N. SALEKI-HASELGHOUBI, M.T. SHERVANI-TABAR, M. TAEIBI-RAHNI, A. DADVAND, *Numerical study on the oscillation of a transient bubble near a confined free surface for droplet generation*, Theor. Comput. Fluid Dyn., **28**, 449–472, 2014.
15. L. RAYLEIGH, *On the pressure developed in a liquid during collapse of a spherical void*, Phil. Mag., **34**, 94–98, 1917.
16. J.P. BEST, *The dynamics of underwater explosions*, PhD Thesis, Department of Mathematics, University of Wollongong, 1–48, 1991.
17. M.T. SHERVANI-TABAR, A. ABDULLAH, M.R. SHABGARD, *Numerical study on the dynamics of an electrical discharge generated bubble in EDM*, Engineering Analysis with Boundary Elements, **30**, 503–514, 2006.
18. A. ZHANG, S. WANG, Z. BAI, C. HUANG, *Experimental study on bubble pulse features under different circumstances*, Acta. Mech. Sin., **43**, 1, 71–83, 2011.
19. A. HAJIZADEH AGHDAM, B.C. KHOO, V. FARHANGMEHR, M.T. SHERVANI-TABAR, *Experimental study on the dynamics of an oscillating bubble in a vertical rigid tube*, Exp. Therm. Fluid. Science, **60**, 299–307, 2015.
20. H. ISHIDA, C. NUNTADUSIT, H. KIMOTO, T. NAKAGAWA, T. YAMAMOTO, *Cavitation bubble behavior near solid boundaries*, Cav. Section, **A5.003**, 2001.

Received September 29, 2014; revised version January 29, 2016.